

# Collective Flavor Oscillations Of Supernova Neutrinos and r-Process Nucleosynthesis

Sovan Chakraborty<sup>\*,a</sup>, Sandhya Choubey<sup>†,b</sup>, Srubabati Goswami<sup>‡,c</sup>, Kamales Kar<sup>\*,d</sup>

*\*Saha Institute of Nuclear Physics,  
1/AF Bidhannagar, Kolkata 700064, India*

*†Harish-Chandra Research Institute,  
Chhatnag Road, Jhansi, Allahabad 211019, India*

*‡Physical Research Laboratory, Navrangpura,  
Ahmedabad 380009, India*

## ABSTRACT

Neutrino-neutrino interactions inside core-collapse supernovae may give rise to collective flavor oscillations resulting in swap between flavors. These oscillations depend on the initial energy spectra, and relative fluxes or relative luminosities of the neutrinos. It has been observed that departure from energy equipartition among different flavors can give rise to one or more sharp spectral swap over energy, termed as splits. We study the occurrence of splits in the neutrino and antineutrino spectra, varying the initial relative fluxes for different models of initial energy spectrum, in both normal and inverted hierarchy. These initial relative flux variations give rise to several possible split patterns whereas variation over different models of energy spectra give similar results. We explore the effect of these spectral splits on the electron fraction,  $Y_e$ , that governs r-process nucleosynthesis inside supernovae. Since spectral splits modify the electron neutrino and antineutrino spectra in the region where r-process is postulated to happen, and since the pattern of spectral splits depends on the initial conditions of the spectra and the neutrino mass hierarchy, we show that the condition  $Y_e < 0.5$  required for successful r-process nucleosynthesis will lead to constraints on the initial spectral conditions, for a given neutrino mass hierarchy.

<sup>a</sup> email: sovan.chakraborty@saha.ac.in

<sup>b</sup> email: sandhya@hri.res.in

<sup>c</sup> email: sruba@prl.res.in

<sup>d</sup> email: kamales.kar@saha.ac.in

# 1 Introduction

Neutrinos from a core-collapse supernova can play an important role in probing both neutrino properties as well as throwing light on the supernova mechanism [1, 2]. Neutrinos emitted during the explosion of core-collapse supernovae (SN) pass through very large density variation of matter and can undergo MSW resonant flavor conversion [3] which can give useful information on neutrino mass hierarchy and the third leptonic mixing angle  $\theta_{13}$ . They are also influenced by the shock wave formed in the SN core and thus carry information about the explosion mechanism [4, 5, 6, 7, 8, 9].

Recently it was realized that a crucial feature in the study of SN neutrinos comes from the collective neutrino-neutrino interaction at very high densities of the core and this may change the emitted flux of different flavors substantially [10]-[42]. The phenomenology of supernova neutrinos with collective effect including Earth matter effect on SN neutrinos [35], prompt SN [31, 32], diffuse neutrino background from SN [43], failed SN [44] as well as CP violation in SN neutrinos [38] has been studied. For a recent review we refer to [45].

It has been shown that effectively the collective evolution of a three-flavor  $(\nu_e, \nu_\mu, \nu_\tau)$  system can be treated like a two flavor  $(\nu_e, \nu_x)$  scenerio, where  $\nu_x$  can be  $\nu_\mu$  or  $\nu_\tau$  or a linear combination of  $\nu_\mu$  and  $\nu_\tau$  [33, 40]. The flavor evolution for this system is driven by the effective mass squared difference  $\Delta m^2$  and the mixing angle  $\theta_{13}$ . This two flavor scenerio which has been extensively studied [20, 25, 26, 29] shows that for inverted hierarchy (IH,  $\Delta m^2 < 0$ ), above a critical energy (split energy  $E_c$ ), the spectrum in both the electron neutrino ( $\nu_e$ ) and antineutrino ( $\bar{\nu}_e$ ) sectors end up with a complete exchange or swap with  $\nu_x$  and  $\bar{\nu}_x$  respectively, this is referred as “spectral swap”. Recently the studies in [41, 42] analyzed the role of equipartition in energy and variation of luminosity and showed the interesting possibility of multiple splits in the supernova neutrino spectrum for IH. Single spectral split for Normal Hierarchy (NH,  $\Delta m^2 > 0$ ) was also reported for certain values of luminosities.

In this paper our goal is to study (a) the impact of spectral splits on the electron fraction ( $Y_e$ ) which is a diagnostic of successful r-process nucleosynthesis in supernova and (b) the inverse problem which is to see if it is possible to put any constraint on the luminosities by demanding the neutron rich condition on  $Y_e$  which is required for synthesis of heavy nuclei.

Though the site for r-process nucleosynthesis is not known definitely, supernovae are considered to be excellent candidates for it. One of the criteria for the rapid nucleosynthesis to take place is that it has to be in a neutron-rich region. With the two competing beta processes  $n + \nu_e \rightarrow p + e^-$  and  $p + \bar{\nu}_e \rightarrow n + e^+$  occurring in the hot bubble and neutrino driven wind region, the minimal condition is that the electron fraction,  $Y_e < 0.5$ . A more realistic constraint may be  $Y_e < 0.45$ .

Effect of MSW neutrino oscillations on r-process nucleosynthesis were considered in [46], and subsequently in a large number of papers. Since r-process is expected to take place in the neutrino driven wind deep inside the supernova, the matter density in these regions obviously are high. Therefore, in order to have MSW effect one requires mass squared difference  $\Delta m^2 \sim 1 \text{ eV}^2$  or higher. Such large values of  $\Delta m^2$  are possible only if one allows for sterile neutrinos. For only active neutrinos, the mass squared differences are of the order of  $10^{-3} \text{ eV}^2$  (atmospheric) and  $10^{-5} \text{ eV}^2$  (solar) only, and the MSW resonance for these are reached at distances far beyond the r-process region. Therefore with only active neutrinos, one expects no effect of MSW oscillations on r-process nucleosynthesis. However, one will have collective effects driven by these active neutrino mass squared differences and these collective flavor oscillations happen very close to the neutrinosphere

– close enough to impact r-process nucleosynthesis. The effect of the collective oscillations on the possibility of getting n-rich region in the hot bubble was studied in [17]. The problem of r-process in the neutrino-wind region with different evolution scenarios was looked into in [47]. With an improved understanding of the spectral splits in the collective oscillations [41, 42], we re-examine the problem of SN r-process using the two flavor basis as mentioned above. In particular, recent papers have shown that (multiple) spectral splits could happen in either or both the neutrino and antineutrino channels, depending on the initial spectral conditions. Since spectral splits can change the neutrino and antineutrino spectra and hence the value of  $Y_e$ , and since these spectral split patterns depend on the initial conditions of the unoscillated spectra, r-process nucleosynthesis can in principle be used to put constraints on the initial spectral conditions. We perform this exercise as a proof of principle, in a simplified framework, in order to illustrate that such constraints indeed exist. We consider different models for the initial neutrino spectrum with different hierarchies among average energies and departures from energy equipartition among flavors. We demonstrate the occurrence of spectral splits due to these variations on the probabilities and the fluxes for both hierarchies. We use the constraint that the environment should be neutrino rich for successful r-process and delineate the resulting constraints that are obtained on the fractional luminosities.

The paper is organized as follows. In Section 2, we outline the neutrino-neutrino interaction in the context of the supernova problem. First the two flavor evolution equations are presented. Next we vary the fractional luminosities for different initial energy spectrum model and study the effect of collective oscillations, especially the effect of the spectral splits on the emitted neutrino flux. In Section 3, we discuss how the evolution of the electron fraction  $Y_e$  is affected by collective oscillations. The value of  $Y_e$  determines the possibility of having r-process nucleosynthesis in the supernova environment. We impose the constraint that the environment should be neutron rich and study the initial relative fluxes or relative luminosities which are allowed under this constraint. Finally Section 4 makes some concluding remarks.

## 2 Two flavor neutrino-neutrino interaction and Supernova

Close to the neutrinosphere, due to the large neutrino density, neutrinos form a background to themselves. This neutrino-neutrino interaction effect is nonlinear and can give rise to collective flavor transition of neutrinos and antineutrinos. In this section we discuss the flavor evolution equations, different models of supernova neutrino spectrum and the impact of the collective effects on the probabilities and the fluxes for both NH and IH.

### 2.1 Two flavor evolution equations of SN Neutrinos

Due to the large neutrino density inside the neutrinosphere, the neutrino-neutrino interactions lead to coherent oscillations of neutrinos of different energies with some average frequency, giving rise to synchronized oscillations. However, there is no effective flavor conversion due to these synchronized oscillations as the effective mixing angle is highly suppressed due to the large MSW potential in the region close to the neutrinosphere. With the neutrino density decreasing outward, bipolar oscillations begin to take place. These oscillations can lead to complete or partial

swapping (spectral split) of the  $\bar{\nu}_e$  ( $\nu_e$ ) and  $\bar{\nu}_x$  ( $\nu_x$ ) spectra depending on their initial luminosities and average energies. Finally, after a few hundred kilometers, the neutrino-neutrino interactions become negligible and it is the MSW transitions which dominate.

As shown in [33, 40] the collective effect due to neutrino-neutrino interaction effectively involves only two flavors of neutrinos ( $\nu_e, \nu_x$ ), while the other flavor ( $\nu_y$ ) does not evolve under this collective potential. Here  $\nu_x$  is a linear combination of  $\nu_\mu, \nu_\tau$  and  $\nu_y$  is the orthogonal combination to  $\nu_x$ . The only way  $\nu_y$  can effect the final neutrino spectrum is by MSW transition which happens at a larger radius of about  $10^{4-5}$  km, well beyond the collective region which is within a few hundred km from the center of the exploding star. Therefore, the effective evolution of the neutrinos is very well described by the two flavor formalism.<sup>1</sup>

The evolution equations in the two-family Bloch vector notation for the polarization vectors of the neutrino ( $\mathbf{P}$ ) and antineutrino ( $\mathbf{P}'$ ) sector are,

$$\dot{\mathbf{P}} = \mathbf{P} \times (\omega \mathbf{B} - \lambda \hat{\mathbf{z}} - \mu \mathbf{D}) , \quad (1)$$

$$\dot{\mathbf{P}}' = \mathbf{P}' \times (-\omega \mathbf{B} - \lambda \hat{\mathbf{z}} - \mu \mathbf{D}) , \quad (2)$$

where the terms involving  $\omega$ ,  $\lambda$  and  $\mu$  are the ones having the vacuum, matter and neutrino-neutrino interaction effects and the frequencies are represented by

$$\mathbf{B} = (-\sin 2\theta, 0, \cos 2\theta)^T , \quad \omega = \frac{\Delta m^2}{2E} , \quad (3)$$

$$\hat{\mathbf{z}} = (0, 0, 1)^T , \quad \lambda = \sqrt{2} G_F N_e , \quad (4)$$

$$\mathbf{D} = \frac{1}{(N_{\nu_e} + N_{\nu_x} + N_{\bar{\nu}_e} + N_{\bar{\nu}_x})} \int dE (n \mathbf{P} - \bar{n} \mathbf{P}') , \quad \mu = \sqrt{2} G_F (N_{\nu_e} + N_{\nu_x} + N_{\bar{\nu}_e} + N_{\bar{\nu}_x}) , \quad (5)$$

respectively.

$\mathbf{D}$  can be defined in terms of the global polarization vectors  $\mathbf{J}$  and  $\bar{\mathbf{J}}$  i.e  $\mathbf{D} = \mathbf{J} - \bar{\mathbf{J}}$ .

Where

$$\mathbf{J} = \frac{1}{(N_{\nu_e} + N_{\nu_x} + N_{\bar{\nu}_e} + N_{\bar{\nu}_x})} \int dE n \mathbf{P} , \quad \bar{\mathbf{J}} = \frac{1}{(N_{\nu_e} + N_{\nu_x} + N_{\bar{\nu}_e} + N_{\bar{\nu}_x})} \int dE \bar{n} \mathbf{P}' .$$

As usual,  $\theta$  and  $\Delta m^2$  are the mixing angle and mass squared difference respectively. In what follows  $\theta_{eff}$  is taken as  $10^{-5}$  and  $|\Delta m^2| = |\Delta m_{31}^2| = |m_3^2 - m_1^2| = 3 \times 10^{-3} \text{ eV}^2$ .  $N_\alpha$ 's represent the total effective number density of the  $\alpha$ th species.

$$N_\alpha = \int dE n_\alpha , \quad (6)$$

---

<sup>1</sup> The MSW  $\mu$ - $\tau$  resonance can occur inside the supernova under certain conditions [54]. Unlike the standard MSW resonances involving the electron flavor, the  $\mu$ - $\tau$  resonance can occur in the inner supernova layers. The effect of  $\mu$ - $\tau$  neutrino refraction and collective three-flavor transformations in supernovae has been considered in [55]. We have ignored these effects in this work.

where,

$$n = n_{\nu_e} + n_{\nu_x} \quad , \quad \bar{n} = n_{\bar{\nu}_e} + n_{\bar{\nu}_x} \quad , \quad (7)$$

$n_\alpha$ 's are the effective number density per unit energy for the  $\alpha$ 'th species of neutrino and can be expressed as [20]

$$n_\alpha(r, E) = \frac{D(r)}{2\pi R_\alpha^2} \frac{L_\alpha}{\langle E_\alpha \rangle} \Psi_\alpha(E) \quad , \quad (8)$$

where  $L_\alpha$  and  $\langle E_\alpha \rangle$  are the luminosity and average energy for the  $\alpha$ th (anti)neutrino species,  $R_\alpha$  is the neutrinosphere radius. The initial flux of the  $\alpha$ th species at the neutrinosphere is given by  $\frac{L_\alpha}{\langle E_\alpha \rangle}$  whereas the initial energy distribution is represented by  $\Psi_\alpha(E)$ .  $D(r)$  denotes the geometrical function in the ‘‘single angle approximation’’ [20] can be expressed as,<sup>2</sup>

$$D(r) = \frac{1}{2} \left( 1 - \sqrt{1 - \left( \frac{R_\alpha}{r} \right)^2} \right)^2 \quad . \quad (9)$$

The matter effect is removed from the evolution equations as the equations are considered in a frame rotating with angular velocity  $-\lambda \mathbf{z}$  [19].<sup>3</sup> In such a frame all the physical observable remain the same. Thus the evolution equations are

$$\dot{\mathbf{P}} = \mathbf{P} \times (\omega \mathbf{B} - \mu \mathbf{D}) \quad , \quad (10)$$

$$\dot{\mathbf{P}}' = \mathbf{P}' \times (-\omega \mathbf{B} - \mu \mathbf{D}) \quad . \quad (11)$$

These are nonlinear coupled equations (due to the 2nd term containing  $\mathbf{D}$ ) and have to be solved numerically. It is evident from the evolution Eqs. (10) and (11) that there are two relevant frequencies, the usual vacuum frequency ( $\omega$ ) and the neutrino-neutrino interaction strength parameter

---

<sup>2</sup>It is well known that the current-current nature of the weak interaction introduces an angular factor in the Hamiltonian because of which the neutrinos from the SN core traveling along different trajectories encounter different neutrino-neutrino interaction potential. These ‘multi angle’ effects may give rise to kinematical decoherence [22] which in turn can wash out the collective features described above. But for spherically symmetric cases ‘‘single angle’’ approximation i.e neutrino-neutrino interactions averaged along a single trajectory seems to be a fine approximation as the ‘multi angle’ decoherence in this case is rather weak against the collective features [23]. We are aware that the extent of kinetic decoherence is initial flux condition dependent and hence some of the initial fluxes that we consider might lead to kinetic decoherence. In [42] the different possible split patterns with varying neutrino luminosities were studied using the ‘‘single angle approximation’’. In this work we study the multiple split patterns for different models of initial supernova neutrino spectrum in the same spirit as [42]. Multi angle study of these possible spectral patterns for different initial supernova neutrino spectrum might give interesting results like the effect of decoherence, but this is beyond the scope of our work.

<sup>3</sup>Note that though the matter potential is mostly rotated away, it may affect the evolution by delaying the collective effect [21] or by some early decoherence [36] or even modifying very low energy (order of 0.1 MeV) split features [29, 30, 2]. These early effects have very little impact on the over all split patterns at the end of the collective region (400 Km) and the low energy split features below 1 MeV are negligible compared to the total spectra. Moreover the matter potential can be accounted for by choosing a matter suppressed hence small effective mixing angle, as we have chosen a  $\theta_{eff} = 10^{-5}$  [23]. So in the subsequent discussions we neglect the above mentioned roles of the matter term and work with a very small  $\theta_{eff}$  to compensate the matter term. We have explicitly checked that the inclusion of the matter term does not change our results.

( $\mu$ ). For our chosen  $\Delta m^2$  the vacuum frequency is

$$\omega = \frac{\Delta m^2}{2E} = \frac{30}{(4E/\text{MeV})} \text{ km}^{-1}. \quad (12)$$

The usual SN neutrino energy considered is in the range of 0 to 50 MeV, as the SN neutrino flux beyond 50 MeV is very small. Hence we use neutrino energy upto 50 MeV for our calculation.

The other frequency ( $\mu$ ) representing neutrino-neutrino interaction is nontrivial, and is given by

$$\mu = \sqrt{2}G_F(N_{\nu_e} + N_{\nu_x} + N_{\bar{\nu}_e} + N_{\bar{\nu}_x}). \quad (13)$$

The Eqs. (6) to (9) imply that contribution of the  $\alpha$ -th species to  $\mu$  is dependent on radial distance ( $r$ ), neutrinosphere radius ( $R_\alpha$ ), initial flux ( $\frac{L_\alpha}{\langle E_\alpha \rangle}$ ) and initial energy distribution ( $\Psi_\alpha(E)$ ). In our analysis, neutrinosphere radius is taken as 10 km whereas other inputs like initial flux and energy distribution depend on the choice of initial neutrino spectrum model. We analyze the evolution for several neutrino spectrum model.

## 2.2 Models of Initial Neutrino Spectrum

In a core-collapse SN, the gravitational binding energy (about a few times  $10^{53}$  erg) is converted to neutrinos and antineutrinos with energies of the order of 10 MeV and gets emitted in the subsequent  $\sim 10$  sec. Initially a neutronization burst comes out consisting of pure  $\nu_e$ s but with only a very small fraction of the total energy and after that the thermal neutrinos and antineutrinos of all three flavors are emitted. For the thermal neutrinos the initial energy distribution is expected to be Fermi-Dirac (FD), but the results of several simulations [48, 49, 50] found that the distribution must be close to pinched thermal spectra [50] i.e. with a deficit on the high energy side compared to FD. Fermi-Dirac(FD) distribution in energy implies

$$\Psi_\alpha^{FD}(E) \propto \frac{\beta_\alpha (\beta_\alpha E)^2}{e^{\beta_\alpha E} + 1}, \quad (14)$$

and for a choice of average energies of different flavors

$$\langle E_{\nu_e} \rangle = 10 \text{ MeV}, \quad \langle E_{\bar{\nu}_e} \rangle = 15 \text{ MeV}, \quad \langle E_{\nu_x} \rangle = \langle E_{\bar{\nu}_x} \rangle = 24 \text{ MeV}, \quad (15)$$

the inverse temperature parameters are [29]

$$\beta_{\nu_e} = 0.315 \text{ MeV}^{-1}, \quad \beta_{\bar{\nu}_e} = 0.210 \text{ MeV}^{-1}, \quad \beta_{\nu_x} = \beta_{\bar{\nu}_x} = 0.131 \text{ MeV}^{-1}. \quad (16)$$

Whereas the pinched spectra for different simulations are parameterized as [50]

$$\Psi_\alpha(E) = \frac{(1 + \zeta_\alpha)^{1+\zeta_\alpha}}{\Gamma(1 + \zeta_\alpha)} \left( \frac{E_\alpha}{\langle E_\alpha \rangle} \right)^{\zeta_\alpha} \frac{\exp\left(-\left(1 + \zeta_\alpha\right)\frac{E_\alpha}{\langle E_\alpha \rangle}\right)}{\langle E_\alpha \rangle}, \quad (17)$$

$\langle E_\alpha \rangle$  is the average energy of  $\nu_\alpha$ , and  $\zeta_\alpha$  is the pinching parameter.

The effective number density for the  $\alpha$ th species per unit energy is given by

$$n_\alpha(r, E) = \frac{D(r)}{2\pi R_\alpha^2} \frac{L_\alpha}{\langle E_\alpha \rangle} \Psi_\alpha(E) . \quad (18)$$

For a specific choice of  $\Psi_\alpha(E)$  the initial flux ( $\phi_\alpha = \frac{L_\alpha}{\langle E_\alpha \rangle}$ ) for the  $\alpha$ th flavor need to be specified and are very crucial input parameters in our study. Supernova models tell us that almost all the gravitational energy released in core collapse supernovae comes out as  $\nu\bar{\nu}$ s of all flavors. Only one or two percent of it goes into the explosion and the electromagnetic radiation emitted in all wavelengths. The total luminosity scales as  $L(t) = L_0(e^{-t/\tau}/\tau)$  but for a first study we take a time-averaged value for it as done in [29] and [42]. One can of course look at the problem for specific instants of time by changing the total luminosity, early times having larger values.

The total SN binding energy released ( $E_B = 3 \times 10^{53}$  erg) is related to the individual flavor luminosities by

$$L_{\nu_e} + L_{\bar{\nu}_e} + 4L_{\nu_x} = \frac{E_B}{\tau} , \quad (19)$$

assuming no distinction between  $\nu_x$  and  $\bar{\nu}_x$ . We also assume a time-independent constant luminosity over the time  $\tau$ . We take  $\tau = 10$  seconds. Thus the initial fluxes of different flavors get constrained by

$$\phi_{\nu_e}^0 \langle E_{\nu_e} \rangle + \phi_{\bar{\nu}_e}^0 \langle E_{\bar{\nu}_e} \rangle + 4\phi_{\nu_x}^0 \langle E_{\nu_x} \rangle = 3 \times 10^{52} . \quad (20)$$

If we denote the ratio between the initial fluxes of different flavors by

$$\phi_{\nu_e}^0 : \phi_{\bar{\nu}_e}^0 : \phi_{\nu_x}^0 = \phi_{\nu_e}^r : \phi_{\bar{\nu}_e}^r : 1 , \quad (21)$$

where  $\phi_{\nu_e}^r, \phi_{\bar{\nu}_e}^r$  are positive numbers, then Eq. (20) can be written as

$$\phi_{\nu_x}^0 (\phi_{\nu_e}^r \langle E_{\nu_e} \rangle + \phi_{\bar{\nu}_e}^r \langle E_{\bar{\nu}_e} \rangle + 4\langle E_{\nu_x} \rangle) = 3 \times 10^{52} . \quad (22)$$

Note that  $\phi_{\nu_e}^r = \frac{\phi_{\nu_e}^0}{\phi_{\nu_x}^0}$ ,  $\phi_{\bar{\nu}_e}^r = \frac{\phi_{\bar{\nu}_e}^0}{\phi_{\nu_x}^0}$  are basically initial relative fluxes. Thus different choices of  $\phi_{\nu_e}^r$  and  $\phi_{\bar{\nu}_e}^r$  imply different relative luminosities or relative fluxes.

Four representative sets for the energy spectra (in terms of  $\langle E_\alpha \rangle$  and the pinching factor  $\zeta_\nu$ ) and flux ratios usually discussed in literature, are given in Table 1. One simulation by the Lawrence Livermore group (LL) [48] and two different simulations by the Garching group (G1, G2) [50] are presented. Recently [41] used another set of ‘‘plausible’’ flux parameters giving rise to multiple splits in the neutrino spectra is also given. We call this ‘G3’. For the LL spectra we use the FD distribution for  $\Psi$  given in Eq. (14). The  $\beta_\alpha$  for LL are given in Eq. (16). For G1, G2 and G3 spectra we use the pinched spectrum defined in Eq. (17). We assume  $\zeta_{\nu_x} = \zeta_{\bar{\nu}_x} = 4$  and  $\zeta_{\nu_e} = \zeta_{\bar{\nu}_e} = 3$  for G1 and G2. For G3 all  $\zeta_\alpha = 3$ .

Note that the LL simulation obtained a large hierarchy  $\langle E_{\nu_e} \rangle < \langle E_{\bar{\nu}_e} \rangle < \langle E_{\nu_x} \rangle \approx \langle E_{\bar{\nu}_x} \rangle$ , and an almost complete equipartition of energy among the flavors. The Garching simulations predict a smaller hierarchy between the average energies, incomplete equipartition, and increased spectral pinching. The differences in the values of these parameters arise from the different physics inputs.

Model	$\langle E_{\nu_e} \rangle$	$\langle E_{\bar{\nu}_e} \rangle$	$\langle E_{\nu_x, \bar{\nu}_x} \rangle$	$\phi_{\nu_e}^r = \frac{\phi_{\nu_e}^0}{\phi_{\nu_x}^0}$	$\phi_{\bar{\nu}_e}^r = \frac{\phi_{\bar{\nu}_e}^0}{\phi_{\nu_x}^0}$
LL	12	15	24	2.00	1.60
G1	12	15	18	0.80	0.80
G2	12	15	15	0.50	0.50
G3	12	15	18	0.85	0.75

Table 1: The parameters of the used primary neutrino spectra models motivated from SN simulations of the Garching (G1, G2) and the Lawrence Livermore (LL) group. We assume  $\zeta_{\nu_x} = \zeta_{\bar{\nu}_x} = 4$  and  $\zeta_{\nu_e} = \zeta_{\bar{\nu}_e} = 3$  for G1 and G2. For G3 all  $\zeta_\alpha = 3$ . For LL we use a pure FD spectrum.

The equipartition of energy implies

$$L_{\nu_e} = L_{\bar{\nu}_e} = L_{\nu_x} . \quad (23)$$

In terms of our notation it means

$$\phi_{\nu_e}^r = \frac{\langle E_{\nu_x} \rangle}{\langle E_{\nu_e} \rangle}; \quad \phi_{\bar{\nu}_e}^r = \frac{\langle E_{\nu_x} \rangle}{\langle E_{\bar{\nu}_e} \rangle} . \quad (24)$$

So complete equipartition for the Garching simulations would imply flux ratios (Table 2) different from the values in Table 1. Recent analyses [42] have shown that the multiple split cases have origin in the departure from energy equipartition.

Actually there is no reason that equipartition should be strictly followed for the energy released

Model	$\phi_{\nu_e}^r = \frac{\phi_{\nu_e}^0}{\phi_{\nu_x}^0}$	$\phi_{\bar{\nu}_e}^r = \frac{\phi_{\bar{\nu}_e}^0}{\phi_{\nu_x}^0}$
G1	1.50	1.20
G2	1.25	1.00
G3	1.50	1.20

Table 2: The flux ratios for the Garching models with equipartition of energy

from a real supernova. In the next subsection we make extensive analysis of this multiple split phenomena with varying initial fluxes, which is equivalent to varying  $\phi_{\nu_e}^r$  and  $\phi_{\bar{\nu}_e}^r$ .

### 2.3 Survival Probability and Flux

As stated above in this subsection we discuss the impact due to the variation of initial relative fluxes ( $\phi_{\nu_e}^r$  and  $\phi_{\bar{\nu}_e}^r$ ) on the final spectrum. The final spectrum is calculated at 400 km as collective effect is expected to vanish at around 400 km. We also analyze this effect for different models of initial neutrino spectrum LL, G1 and G3.

In principle the values of  $\phi_{\nu_e}^r$  and  $\phi_{\bar{\nu}_e}^r$  can lie in a large range. Thus analysing this variation would require study in a wide range of the  $\phi_{\nu_e}^r$ - $\phi_{\bar{\nu}_e}^r$  parameter space. Instead we consider the

suggestion [51] that the uncertainty in the relative luminosities of different flavors must be in the range

$$\frac{1}{2} \leq \frac{L_{\nu_e}}{L_{\nu_x}} \leq 2 \quad ; \quad \frac{1}{2} \leq \frac{L_{\bar{\nu}_e}}{L_{\nu_x}} \leq 2 . \quad (25)$$

These limits in turn will put a constraint on the parameters  $\phi_{\nu_e}^r$  and  $\phi_{\bar{\nu}_e}^r$

$$\frac{1}{2} \frac{\langle E_{\nu_x} \rangle}{\langle E_{\nu_e} \rangle} \leq \phi_{\nu_e}^r \leq 2 \frac{\langle E_{\nu_x} \rangle}{\langle E_{\nu_e} \rangle} \quad ; \quad \frac{1}{2} \frac{\langle E_{\nu_x} \rangle}{\langle E_{\bar{\nu}_e} \rangle} \leq \phi_{\bar{\nu}_e}^r \leq 2 \frac{\langle E_{\nu_x} \rangle}{\langle E_{\bar{\nu}_e} \rangle} . \quad (26)$$

In Table 3 we present the lower limits (ll) and upper limits (ul) of the initial relative fluxes for different spectrum models LL, G1 and G3.

Model	$\langle E_{\nu_e} \rangle$	$\langle E_{\bar{\nu}_e} \rangle$	$\langle E_{\nu_x, \bar{\nu}_x} \rangle$	$\phi_{\nu_e;ll}^r$	$\phi_{\nu_e;ul}^r$	$\phi_{\bar{\nu}_e;ll}^r$	$\phi_{\bar{\nu}_e;ul}^r$
LL	10	15	24	1.20	4.80	0.80	3.2
G1	12	15	18	0.75	3.00	0.60	2.4
G3	12	15	18	0.75	3.00	0.60	2.4

Table 3: The average energies, upper limits (ul) and lower limits (ll) of the initial relative flux for the models used.

To compare different flux models and study more of the parameter space we vary  $\phi_{\nu_e}^r$  and  $\phi_{\bar{\nu}_e}^r$  in the range [0.5,5.0] and [0.5,3.5] respectively, for all the models. We find that varying  $\phi_{\nu_e}^r$  and  $\phi_{\bar{\nu}_e}^r$  give rise to different possibilities of final spectra as discussed in [42]. In addition to that we check it for different initial spectrum models. Here it is notable that usually the initial spectrum models come with a fixed value of  $\phi_{\nu_e}^r$  and  $\phi_{\bar{\nu}_e}^r$  (see Table 1) but the main idea in this analysis is about varying  $\phi_{\nu_e}^r$  and  $\phi_{\bar{\nu}_e}^r$ . So here by initial spectrum models (like LL, G1, G3) we mean the energy dependence ( $\zeta_{\nu_\alpha}$ ) and neutrino average energies ( $\langle E_{\nu_\alpha} \rangle$ ) of the models. In what follows, we will see that for the Inverted Hierarchy (IH) the final spectrum is very sensitive to the values of  $\phi_{\nu_e}^r$ ,  $\phi_{\bar{\nu}_e}^r$  and the model of initial spectrum. Whereas for Normal Hierarchy (NH), the results are less dependent on these quantities. We will discuss the reasons for this behavior.

### 2.3.1 Probability and Flux: NH

As already discussed in [41, 42], large flux (luminosity) of  $\nu_x$  can induce simultaneous swap in both neutrino and antineutrino sector for NH. In these cases initially the system is in an unstable equilibrium. As it evolves, it partially swaps the flavor in both neutrino as well as antineutrinos, to end up in a stable state. We further study this over different spectrum models and initial relative fluxes. For each of the different models we vary  $\phi_{\nu_e}^r$  and  $\phi_{\bar{\nu}_e}^r$  in the range [0.5,5.0] and [0.5,3.5] respectively. We find that for several choices of  $(\phi_{\nu_e}^r, \phi_{\bar{\nu}_e}^r)$  there is simultaneous swap in both neutrino and antineutrino spectrum and this swap may generate prominent split in the final spectrum. For a specific model these split energies ( $E_c$ ) may vary from low to high energies, depending on the value of  $(\phi_{\nu_e}^r, \phi_{\bar{\nu}_e}^r)$ .

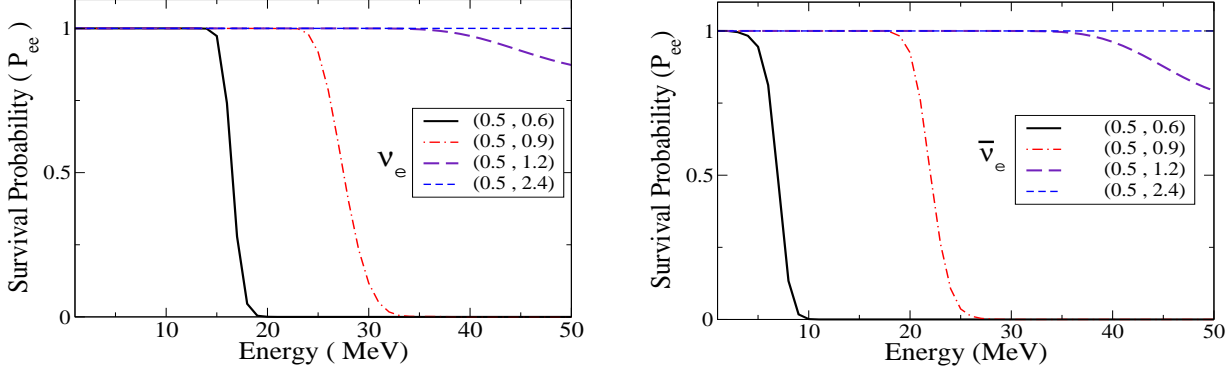


Figure 1: Survival probability for G3 spectrum in NH with different  $(\phi_{\nu_e}^r, \phi_{\bar{\nu}_e}^r)$ .

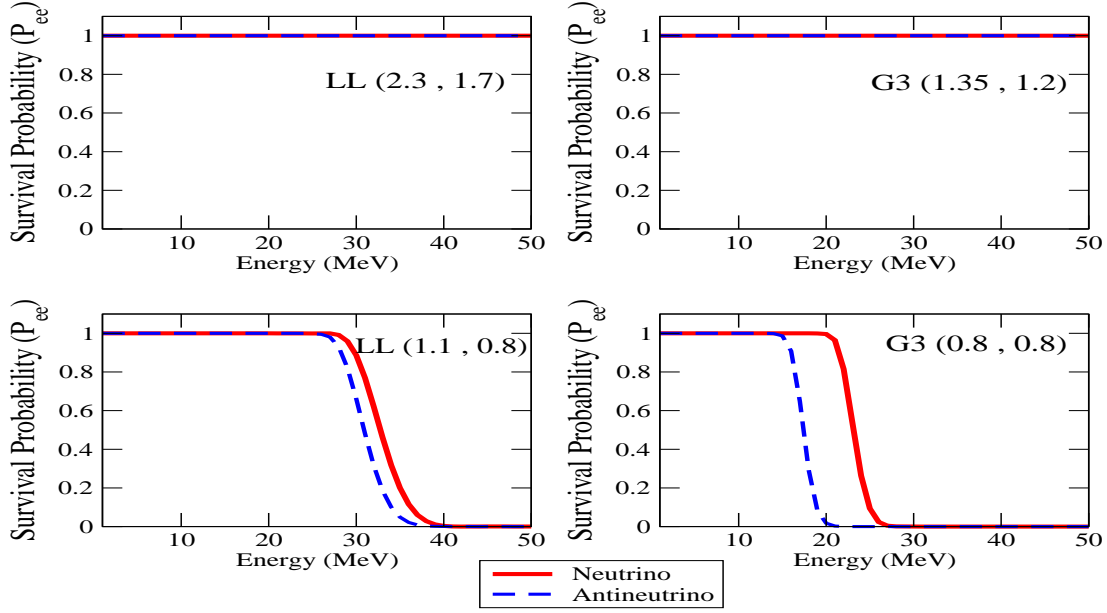


Figure 2: Survival probability for LL and G3 spectrum in NH with different  $(\phi_{\nu_e}^r, \phi_{\bar{\nu}_e}^r)$ .

Independent of the choice of spectrum models, these split features are seen for low values of  $(\phi_{\nu_e}^r, \phi_{\bar{\nu}_e}^r)$ , which implies large flux of  $\nu_x$  compared to other flavors [42]. As the values of  $(\phi_{\nu_e}^r, \phi_{\bar{\nu}_e}^r)$  increase, the split energy ( $E_c$ ) also increases, and close to the equipartition point the split energy tends to infinity.

As an example see Figure 1 where survival probabilities are plotted for the spectrum G3. The left panel is for neutrino and right one for antineutrino. For a low value of  $\phi_{\nu_e}^r$  (0.5),  $\phi_{\bar{\nu}_e}^r$  is increased from 0.6 to 2.4 for both neutrino and antineutrino. From the figures it is evident that with this increment, split energies ( $E_c$ ) also increase. For the same combination of  $\phi_{\nu_e}^r$  and  $\phi_{\bar{\nu}_e}^r$  the split energy is higher for neutrinos than for antineutrinos. We find these features are same for other spectrum models too.

In Figure 2 we have shown the above mentioned features for LL and G3. The left panels are for LL and the right ones are for G3. The red straight lines are for neutrino and the blue dashed lines

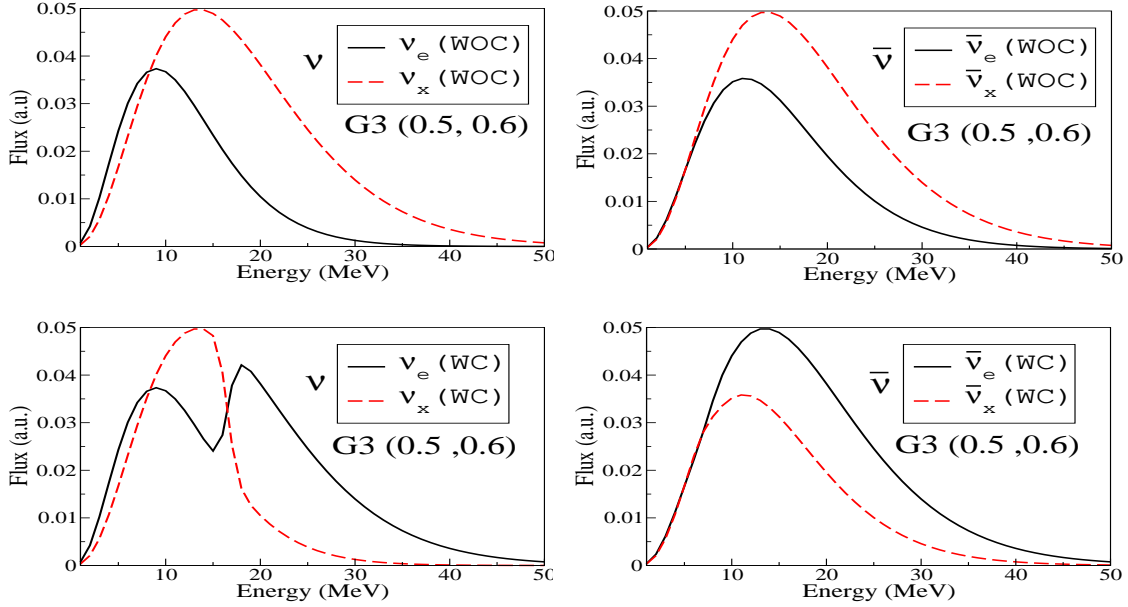


Figure 3: Flux for the different neutrino species for G3 with NH in arbitrary units (a.u.); WOC stands for “Without Collective” effects and WC for “With Collective” effects.

are for antineutrino. In the top panels the initial relative spectrum ( $\phi_{\nu_e}^r, \phi_{\bar{\nu}_e}^r$ ) are chosen to be close to the equipartition point for both the models and for these values there is no split whereas for the lower panels ( $\phi_{\nu_e}^r, \phi_{\bar{\nu}_e}^r$ ) are smaller and these panels show split for both neutrino and antineutrino sectors.

The flux corresponding to G3 and (0.5,0.6) are plotted in Figure 3. Left and right panels in this figure are respectively for neutrinos and antineutrinos. The upper panels are without collective effects (initial flux) and the lower ones are with collective effect (flux beyond collective region). The black lines in the panels are for electron type whereas the red dashed lines are for x-type. Clearly the lower panels show swap in both neutrino and antineutrino sector. The swap in both sectors are partial, that is, a part of the spectra below the “split energy” remains same. The antineutrino split feature is not clearly visible since  $E_c$  for them is low and the  $\bar{\nu}_e$  and  $\bar{\nu}_x$  fluxes are very close to each other at these energies. The probability plots for (0.5,0.6) in Figure 1 also show the low split energy for antineutrino. Note that the swap for neutrino spectra happens at a higher energy compared to the antineutrino spectra, this feature is also consistent with the probability plots in Figure 1.

### 2.3.2 Probability and Flux: IH

Probability and flux in the IH is much more complex and interesting than NH. Here also we vary the initial relative flux for different spectrum models and find wide variation of the final spectrum depending on the choice of ( $\phi_{\nu_e}^r, \phi_{\bar{\nu}_e}^r$ ). These variations in spectrum with initial relative flux ( $\phi_{\nu_e}^r, \phi_{\bar{\nu}_e}^r$ ) have been attributed to meeting the instability condition of the initial system and adiabaticity violation [41] as well as to change of global initial condition with luminosity variation and minimization of potential energy [42]. We find that these changes in final spectrum are similar

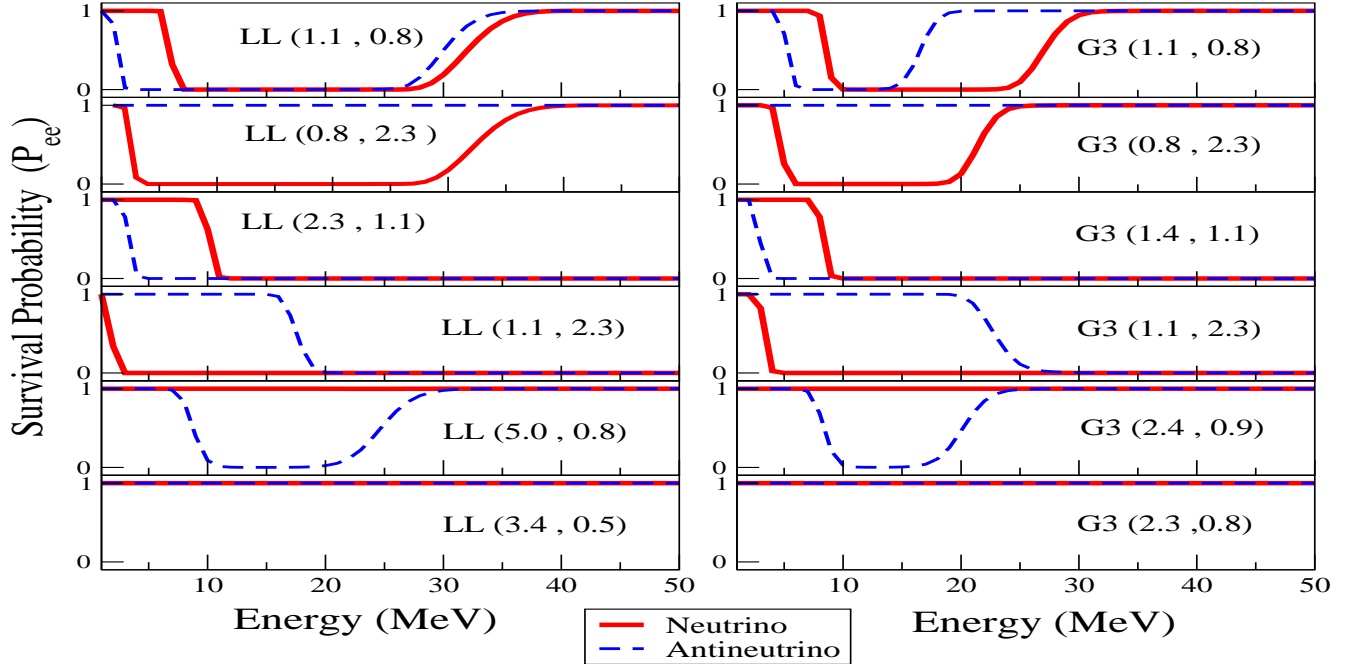


Figure 4: Survival Probability for LL and G3 spectrum in IH with different  $(\phi_{\nu_e}^r, \phi_{\bar{\nu}_e}^r)$ .

for different choices of spectrum models.

As discussed in [42], the different spectral features arise from the initial conditions, which may or may not lead the system to swap to minimize “potential energy”. We also find that in some cases the multiple swaps actually do take place but the swaps are so close that they can not be resolved numerically [41] and thus appear as if the swap or split features are absent. We find five spectral split patterns as mentioned in [42]. These five patterns are found for all three models of initial energy spectra LL, G1, G3. These are displayed (for LL and G3) in successive panels from top to bottom in Figure 4.

1. Dual split in both neutrino and antineutrino flux (II,II).
2. Dual split in neutrino but no split in antineutrino flux (II,0).
3. One split in both neutrino and antineutrino flux with the split energy of the neutrino higher (H) than that of antineutrino (L) split energy (I,I)(H,L).
4. One split in both neutrino and antineutrino flux with the split energy of the neutrino lower (L) than that of antineutrino (H) split energy (I,I)(L,H).
5. No split in neutrino but dual split in antineutrino flux (0,II).

Apart from these five patterns we find a sixth possible pattern in which neither neutrino nor antineutrino show any swap in the spectrum. We call this (0,0). For this pattern (0,0) the effect of neutrino-neutrino interaction on both neutrino and anti neutrino flux is undetectable.

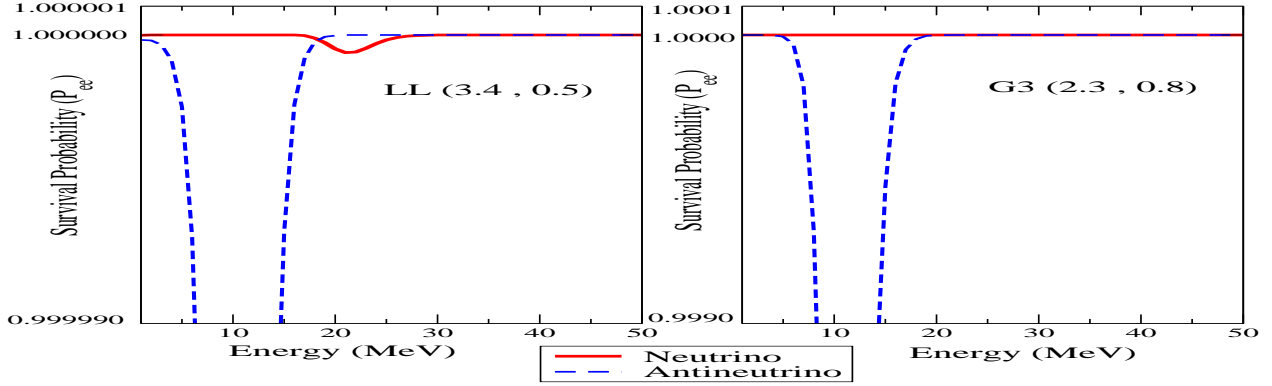


Figure 5: Survival Probability for LL (3.4, 0.5) and G3 (2.3, 0.8) spectrum in IH .

The physical reasoning behind the patterns in the top five panels are well explained [42] from the idea of potential energy minimization. Our analysis shows that in some sense all the different spectrum models are in the same footing as all of them give rise to similar split patterns with the change of initial relative flux or relative luminosity. As explained in [41] the basic feature is that there are multiple swaps or splits in both the neutrino and antineutrino sector but the swaps may disappear depending on the adiabaticity violation or it may be numerically unresolvable. split patterns Consider the new pattern, described in the lowest panel of Figure 4, where it seems that there is no swap in both neutrino and antineutrino sectors. When we study these cases carefully (Figure 5, left panel LL (3.4,0.5) and right panel G3 (2.3,0.8)) we find that they also show changes in survival probability similar to the other patterns. But the swaps here are incomplete and numerically undetectable. While in Figure 4 the change in probability for this case is visually unresolvable for all practical purposes, in Figure 5 it is visible, as we have increased the resolution.

For the fluxes we just give one example of the case (II,II) in Figure 6. Here we plotted the G3 neutrino spectrum in the left panel and the G3 antineutrino spectrum in right one. In both panels, the solid sky blue lines are for electron type without collective effect (WOC) and the solid red lines are for  $\nu_x$  without collective effect (WOC). For the spectrum with collective effects (WC) dashed black lines are for electron type whereas dot-dashed blue lines are for  $\nu_x$ . Here the spectrum model used is G3 and the initial relative fluxes are (1.1,0.8). We can see prominent dual split pattern in this flux figure as expected from the upper right panel of Figure 4.

Thus, depending upon the choice of initial relative fluxes ( $\phi_{\nu_e}^r, \phi_{\bar{\nu}_e}^r$ ) the spectra can have different patterns, especially for IH. The possible values of ( $\phi_{\nu_e}^r, \phi_{\bar{\nu}_e}^r$ ) can be in a wide range. Even if one assumes a factor-of-two-uncertainty in the relative luminosity [51], there can be considerable variations in the final flux characteristics.

We study the variation in spectral split features over the  $\phi_{\nu_e}^r - \phi_{\bar{\nu}_e}^r$  plane for LL, G1, G3 and found a pattern showing different kind of spectral splits at different  $\phi_{\nu_e}^r - \phi_{\bar{\nu}_e}^r$  region. In Figure 7 we show this in the  $\phi_{\nu_e}^r - \phi_{\bar{\nu}_e}^r$  plane. The plane is divided into zones by the values of the global polarization vectors  $J_z, \bar{J}_z$  and  $D_z$ . The black dashed line divides the plane into zones with  $D_z > 0$  and  $D_z < 0$ . The purple long dashed corresponds to  $\bar{J}_z = 0$  and demarcates the area which has  $\bar{J}_z$  positive and negative. The blue thick dashed is for  $J_z = 0$ . These lines therefore divide the  $\phi_{\nu_e}^r - \phi_{\bar{\nu}_e}^r$

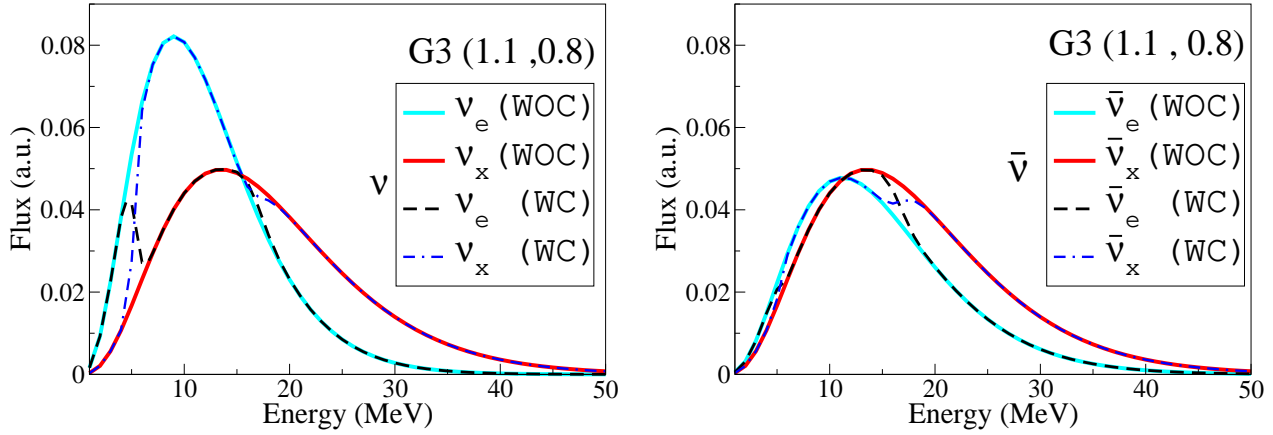


Figure 6: The neutrino and antineutrino fluxes in arbitrary units (a.u.) for the model G3 with the relative luminosities (1.1,0.8), with and without collective effect for IH.

plane into 6 zones. The split patterns observed in the different zones are shown on the plane. The global polarization vectors  $J_z$ ,  $\bar{J}_z$  and  $D_z$ , define the “phase transitions” across different split patterns. It should be noted that the global polarization vectors were initially in the z direction hence the sign changes of their z components mark the stability of the system and spectral splits [42]. Figure 7 shows that

1. (I,I)(H,L) patterns are for  $J_z > 0$ ,  $\bar{J}_z > 0$  and  $D_z > 0$ ,
2. (I,I)(L,H) for  $J_z > 0$ ,  $\bar{J}_z > 0$  and  $D_z < 0$ ,
3. (a) (II,II) patterns are seen in the  $J_z < 0$ ,  $\bar{J}_z < 0$  region, and also in the  $J_z > 0$ ,  $\bar{J}_z < 0$  region,  
 (b) (0,0) appear mostly in  $\bar{J}_z < 0$  with a very few occurrence in  $J_z < 0$ ,  
 (c) (II,0) is the most dominant pattern in the  $J_z < 0$  region, although it can appear in the  $J_z > 0$ ,  $\bar{J}_z < 0$  region,  
 (d) (0,II) pattern occurs only in  $\bar{J}_z < 0$ .

Thus for the double split patterns described in point 3 above, the so called “phase transition” lines seems inconclusive. [42] established that the  $J_z < 0$  or  $\bar{J}_z < 0$  region (i.e, the rectangle covering the zone with  $J_z < 0$  alongwith the rectangle covering the zone with  $\bar{J}_z < 0$  ) lead to (II,II) pattern when the adiabaticity is increased artificially. Hence due to the incomplete adiabaticity in the actual case some of the (II,II) patterns appear as (II,0), (0,II), (0,0) pattern. So with complete adiabaticity one will not see any of the (II,0), (0,II), (0,0) patterns in Figure 7. For example see the discussion regarding the (0,0) pattern in context of Figure 4.

With so many possible patterns it will be really difficult to predict the initial relative neutrino fluxes, the energy distribution model and the extent of collective neutrino effect, even for a future galactic supernova event. In the next section we discuss to what extent one can constrain the

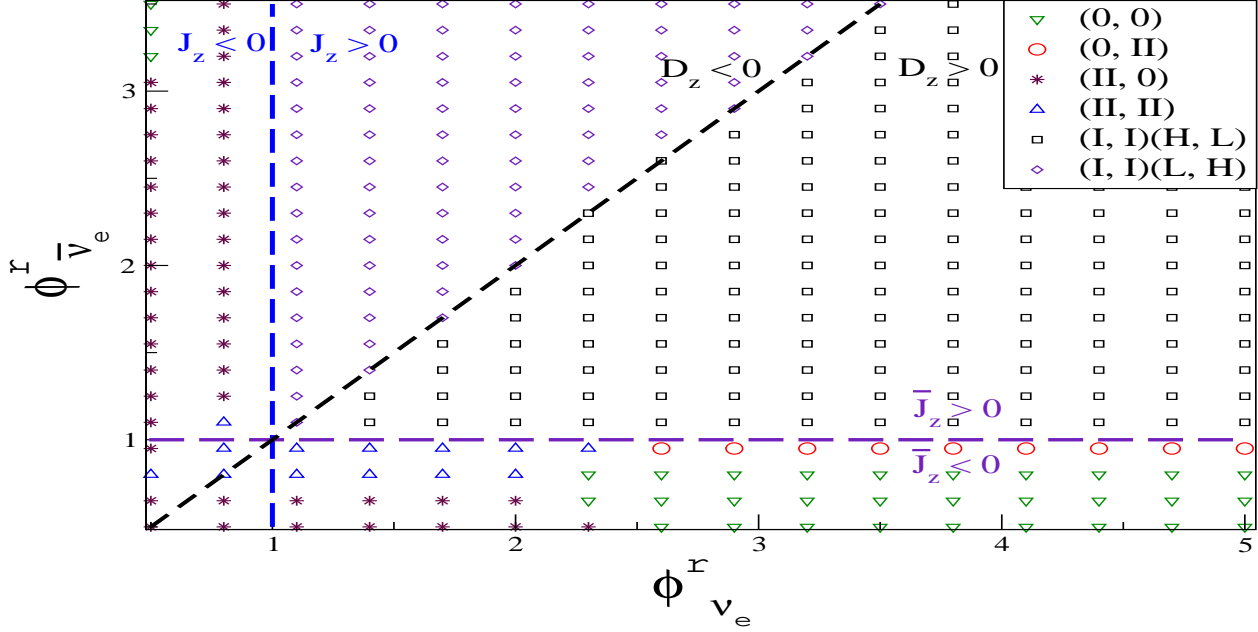


Figure 7: The different split pattern regions in the  $\phi_{\nu_e}^r - \phi_{\bar{\nu}_e}^r$  plane for IH and G3. The black dashed, purple long dashed, blue thick dashed denotes  $D_z = 0$ ,  $\bar{J}_z = 0$  and  $J_z = 0$  lines respectively. The six zones in  $\phi_{\nu_e}^r - \phi_{\bar{\nu}_e}^r$  plane have different split patterns. The abbreviations used are explained in section 2.3.2.

luminosities by demanding a neutron rich condition by the end of the collective region, required for successful r-process.

### 3 Neutrino Fluxes and r-Process Nucleosynthesis

In this section we discuss the effect of the flux of neutrinos radiated out in core collapse supernovae on the electron fraction and discuss the possibility of getting allowed regions for r-process nucleosynthesis and the resulting constraints on relative luminosities. As most simulations of core-collapse supernovae do not lead to explosions, there are uncertainties in the understanding of the late stage of the SN shock propagation. But the generally accepted scenario supported by simulations is that for core collapse supernovae starting with iron cores the shock wave gets initially stalled due to loss of energy through nuclear dissociation and then over timescale of a second, gets revived by the energy deposited by neutrinos radiating out, the so-called late-time neutrino heating mechanism leading to the delayed core collapse supernova [52]. This results in the development of a low density “hot bubble” region just behind the SN shock. Normally the hot bubble regions are taken between the infalling neutron star radius and the forward shock, that is, up to 30-40 km initially. The huge flux of neutrinos emitted from the proto-neutron star leads to the “neutrino-driven wind” which remains active for about 10 seconds after the core bounce. This creates neutron-rich regions of high entropy which are conducive to the development of the r-

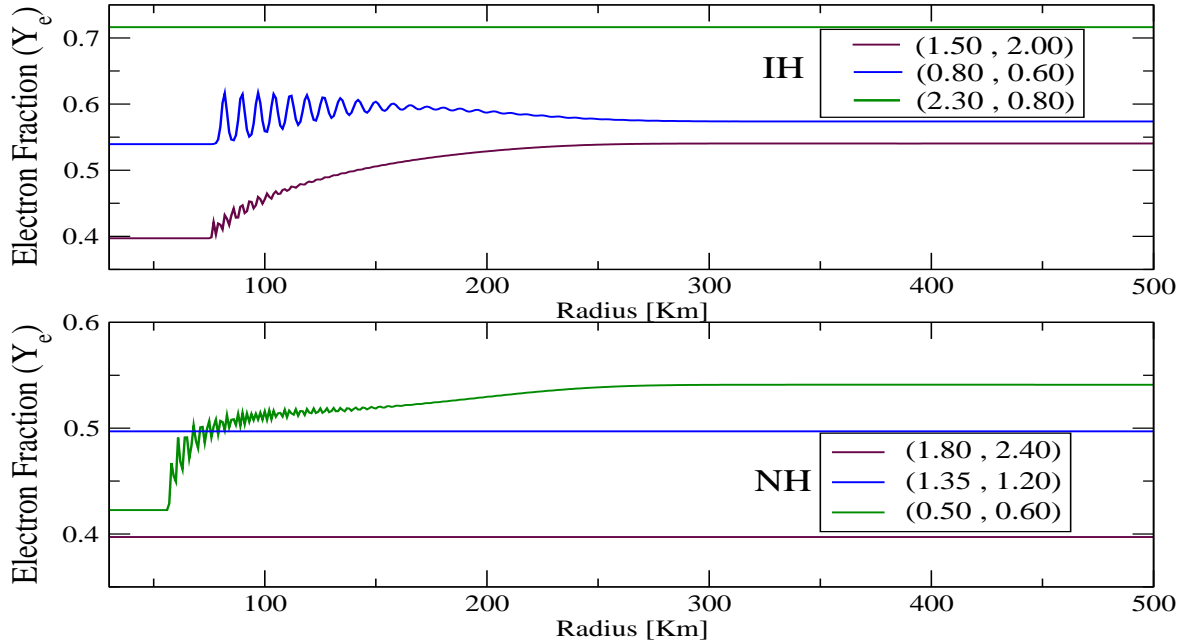


Figure 8: The electron fraction  $Y_e$  for both hierarchies as a function of ‘r’, the distance of the region from the center of the core. The spectrum model used is G3.

process. Different delayed core-collapse SN calculations give rise to different values for the entropy per baryon leading to conflicting conclusions about the r-process. However the  $\nu$ -driven wind is still considered to be one of the most probable sites for the r-process [52]. The  $\nu$ -driven wind models consider the r-process site to be at a few hundred kilometers (within 1000 km) [52]. Since, as discussed before, this is also the region where collective oscillations are active, it is expected that r-process will get affected. In what follows, we study this effect in the  $\nu$ -driven wind region and numerically check if criteria of successful r-process can be used to constrain initial neutrino flux parameters.

The criteria for r-process on which we focus here is the the electron fraction  $Y_e$ , *i.e.*, the number of electrons (equal to the number of protons, due to charge neutrality) per baryon. The  $Y_e$  will depend on the relative strengths of the two reactions – neutrino capture on neutrons and antineutrino capture on protons. Therefore,  $Y_e$  can be expressed as [46]

$$Y_e = 1/(1 + \lambda_{\bar{\nu}_e p}/\lambda_{\nu_e n}) , \quad (27)$$

where  $\lambda_{\nu_e n}$  and  $\lambda_{\bar{\nu}_e p}$  are the reaction rates for  $\nu_e + n \rightarrow e^- + p$  and  $\bar{\nu}_e + p \rightarrow e^+ + n$  respectively. Note that these reactions can in principle occur on both free and bound nucleons. However for the purpose of this work, we will not consider the reactions on heavy nuclei<sup>4</sup>. Note also that

<sup>4</sup>For a detailed study of the effect of nuclear compositions on  $Y_e$  we refer to [16]. Our main conclusions come

in principle, the inverse reactions also happen inside the supernova and should be considered. However, we neglect the inverse reactions here since the matter temperature of the region is small compared to the neutrino temperature as one goes away from the neutrinosphere and has very small effect at radius of 30 km and beyond [46, 53]. The reaction rates  $\lambda_{\nu N}$  (where  $N = n$  or  $p$ ) are given as

$$\lambda_{\nu N} \approx \frac{L_\nu}{4\pi r^2} \frac{\int_0^\infty \sigma_{\nu N}(E) f_\nu(E) dE}{\int_0^\infty E f_\nu(E) dE}, \quad (28)$$

where  $L_\nu = \phi_\nu^0 \langle E_\nu \rangle$ , and  $f_\nu$  denotes the neutrino flux. The cross section used are

$$\sigma_{\nu_e n}(E_{\nu_e}) \approx 9.6 \times 10^{-44} \left( \frac{E_{\nu_e} + \Delta_{np}}{\text{MeV}} \right)^2 \text{ cm}^2, \quad (29)$$

$$\sigma_{\bar{\nu}_e p}(E_{\bar{\nu}_e}) \approx 9.6 \times 10^{-44} \left( \frac{E_{\bar{\nu}_e} - \Delta_{np}}{\text{MeV}} \right)^2 \text{ cm}^2, \quad (30)$$

where  $\Delta_{np} = 1.293$  MeV is the mass difference between neutron and proton.

Note that the neutrino flux denoted as  $f_\nu$  in Eq. (28) is the flux including collective flavor oscillations. The swap between the active neutrinos due to collective effect can change  $f_\nu$  and hence  $Y_e$ . To illustrate this better we show the ratio of the reaction rates for  $\bar{\nu}_e$  and  $\nu_e$  explicitly in terms of the collective oscillation probabilities

$$\frac{\lambda_{\bar{\nu}_e p}}{\lambda_{\nu_e n}}(r) = \frac{\int_0^\infty \sigma_{\bar{\nu}_e p}(E) P_{\bar{\nu}_e}^c(r, E) \phi_{\bar{\nu}_e}^r \Psi_{\bar{\nu}_e}(E) dE + \int_0^\infty \sigma_{\bar{\nu}_e p}(E) (1 - P_{\bar{\nu}_e}^c(r, E)) \Psi_{\nu_x}(E) dE}{\int_0^\infty \sigma_{\nu_e n}(E) P_{\nu_e}^c(r, E) \phi_{\nu_e}^r \Psi_{\nu_e}(E) dE + \int_0^\infty \sigma_{\nu_e n}(E) (1 - P_{\nu_e}^c(r, E)) \Psi_{\nu_x}(E) dE}, \quad (31)$$

where  $P_{\bar{\nu}_e}^c(r, E)$  and  $P_{\nu_e}^c(r, E)$  are the anti-neutrino and neutrino survival probabilities with collective oscillations and are calculated numerically as function of radius and energy. The minimal condition for the SN environment to become neutron rich is  $Y_e < 0.5$  which translate as the condition  $\lambda_{\bar{\nu}_e p} / \lambda_{\nu_e n} > 1$ .

Let us begin by understanding the impact of collective flavor oscillations on r-process by discussing some limiting cases. In the no flavor oscillation limit, i.e.  $P_{\bar{\nu}_e}^c = P_{\nu_e}^c = 1.0$  for all energies, Eq. (31) reduces to

$$\left( \frac{\lambda_{\bar{\nu}_e p}}{\lambda_{\nu_e n}} \right)_{\text{no osc}} \simeq \frac{\phi_{\bar{\nu}_e}^r \int_0^\infty (E - \Delta_{np})^2 \Psi_{\bar{\nu}_e}(E) dE}{\phi_{\nu_e}^r \int_0^\infty (E + \Delta_{np})^2 \Psi_{\nu_e}(E) dE} \simeq \frac{\phi_{\bar{\nu}_e}^r \langle (E - \Delta_{np})^2 \rangle_{\bar{\nu}_e}}{\phi_{\nu_e}^r \langle (E + \Delta_{np})^2 \rangle_{\nu_e}} \quad (32)$$

Since the average energy of  $\bar{\nu}_e$  is greater than that of  $\nu_e$  for all the three SN models that we have considered, it is expected that  $\langle (E - \Delta_{np})^2 \rangle_{\bar{\nu}_e} > \langle (E + \Delta_{np})^2 \rangle_{\nu_e}$ . Therefore under this approximation, for  $\phi_{\bar{\nu}_e}^r / \phi_{\nu_e}^r \geq 1$ ,  $Y_e < 0.5$  always and r-process can proceed. The condition  $Y_e \leq 0.5$  in fact gives  $\phi_{\bar{\nu}_e}^r / \phi_{\nu_e}^r \geq 0.62$  for LL and  $\geq 0.88$  for G1/G3. For all values of  $\phi_{\bar{\nu}_e}^r / \phi_{\nu_e}^r$  greater than this value, r-process can happen while for all values of  $\phi_{\bar{\nu}_e}^r / \phi_{\nu_e}^r$  below this, r-process is forbidden.

---

from impact of collective oscillations on r-process nucleosynthesis and are not expected to drastically change as a result of reactions on bound nucleons.

Likewise one could consider the case where we have complete conversion of both neutrinos and antineutrinos where  $P_{\bar{\nu}_e}^c = P_{\nu_e}^c = 0$  for all energies. One can easily show that for this case  $\lambda_{\bar{\nu}_e p}/\lambda_{\nu_e n} = \langle (E - \Delta_{np})^2 \rangle_{\nu_x} / \langle (E + \Delta_{np})^2 \rangle_{\nu_x}$ . As a result here one always gets  $Y_e > 0.5$  as  $\Delta_{np}$  is positive. Note however that this case never happens in collective oscillations and is therefore not realistic.

Next we consider effect of collective effects on r-process for the realistic case, where the flavor conversions are calculated numerically, as outlined in the previous section. In Figure 8 we show the electron fraction  $Y_e$  as a function of the radius ( $r$ ), for different combinations of  $\phi_{\nu_e}^r$  and  $\phi_{\bar{\nu}_e}^r$ . We have taken the G3 model for the  $\nu_e$  and  $\bar{\nu}_e$  spectra. The upper panel is for IH while the lower one is for NH. In the upper panel, the green line is for  $(\phi_{\nu_e}^r, \phi_{\bar{\nu}_e}^r)$  of (1.5, 2.0), the blue line for (0.8, 0.6), while the maroon line is for (2.3, 0.8). We can note from the figure that for IH and (2.3, 0.8) case, there is no flavor conversion due to oscillations for the inverted hierarchy. The probability  $P_{\bar{\nu}_e}^c$  and  $P_{\nu_e}^c$  for this case was shown in the lowest right-hand panel of Figure 4, where we can see that  $P_{\bar{\nu}_e}^c = P_{\nu_e}^c = 1$ . Therefore as discussed above, the  $\lambda_{\bar{\nu}_e p}/\lambda_{\nu_e n} = (0.8/2.3) * \langle (E - \Delta_{np})^2 \rangle_{\bar{\nu}_e} / \langle (E + \Delta_{np})^2 \rangle_{\nu_e} = 0.396$ , giving  $Y_e \sim 0.72$ . For the two other cases considered with IH we have oscillations due to single and multiple splits. A scan of Figure 7 reveals that we have double splits in both neutrino and antineutrino channels for the blue line with (0.80, 0.60) whereas for the maroon lines of (1.50, 2.00) we have single splits in both neutrino and antineutrino channels with the split energy of neutrino lower than that of antineutrino. For both these cases we can see very fast oscillations in  $Y_e$  within the first 200 km, which can be attributed to the bipolar collective oscillations. Beyond 300 km the value of  $Y_e$  approaches a fixed value as the neutrino density decreases very fast and the collective effects end. The reason that one gets higher values of  $Y_e$  for both of them after the completion of collective effects compared to their values at 30 km can become clear from Eq. (31). For double splits for fixed value of  $\phi_{\bar{\nu}_e}^r/\phi_{\nu_e}^r$  the contribution from the integrals in denominator in between the split energies is more than the corresponding contribution in the numerator making the ratio lower, resulting in higher  $Y_e$ . On the other hand for the single split case of (1.50, 2.00) the low split energies in the denominator for neutrinos make the ratio of Eq. (31) lower.

In the lower panels we assume NH and show  $Y_e$  for (0.5, 0.6) by the green line, for (1.35, 1.2) by the blue line, and (1.8, 2.4) by the maroon line. For the (1.35, 1.2) case, we had noted before in Figure 2, that  $P_{\bar{\nu}_e}^c = P_{\nu_e}^c = 1$  over the entire energy range. For the case (1.8, 2.4) there is no conversion as well. Hence for these case there is no flavor conversion and  $Y_e$  stays constant for all  $r$ , given solely in terms of the  $\phi_{\bar{\nu}_e}^r/\phi_{\nu_e}^r$  and  $\langle (E - \Delta_{np})^2 \rangle_{\bar{\nu}_e} / \langle (E + \Delta_{np})^2 \rangle_{\nu_e}$  ratios. For the case (0.5, 0.6) (cf. Figure 1) we have single split in both the neutrino and antineutrino channels. For this case therefore we see a variation in  $Y_e$  as a function of the radius. Since we have noted that for cases of  $(\phi_{\nu_e}^r, \phi_{\bar{\nu}_e}^r)$  for which there is flavor conversion due to collective effects,  $Y_e$  fluctuates non-trivially with the radius for  $r \lesssim 400$  km, therefore in what follows, we will show all results for  $r \gtrsim 400$  km. That implies that we consider only the neutrino-driven wind region henceforth.

Figure 8 also shows the most significant aspect of flavor conversion due to collective effects. At  $r = 30$  km, one is in the synchronization phase and the collective bipolar oscillations are yet to set in. This is the limiting case of no conversion already discussed, while by  $r = 400$  km, they are complete. The maroon line (1.5, 2.0) for IH and green line (0.5, 0.6) for NH show that collective effects can change the value of the electron fraction from  $Y_e < 0.5$  (at  $r = 30$  km) to  $Y_e > 0.5$  (at  $r = 400$  km). Hence, we can explicitly see that these combination of values of  $\phi_{\nu_e}^r$  and  $\phi_{\bar{\nu}_e}^r$  (for the

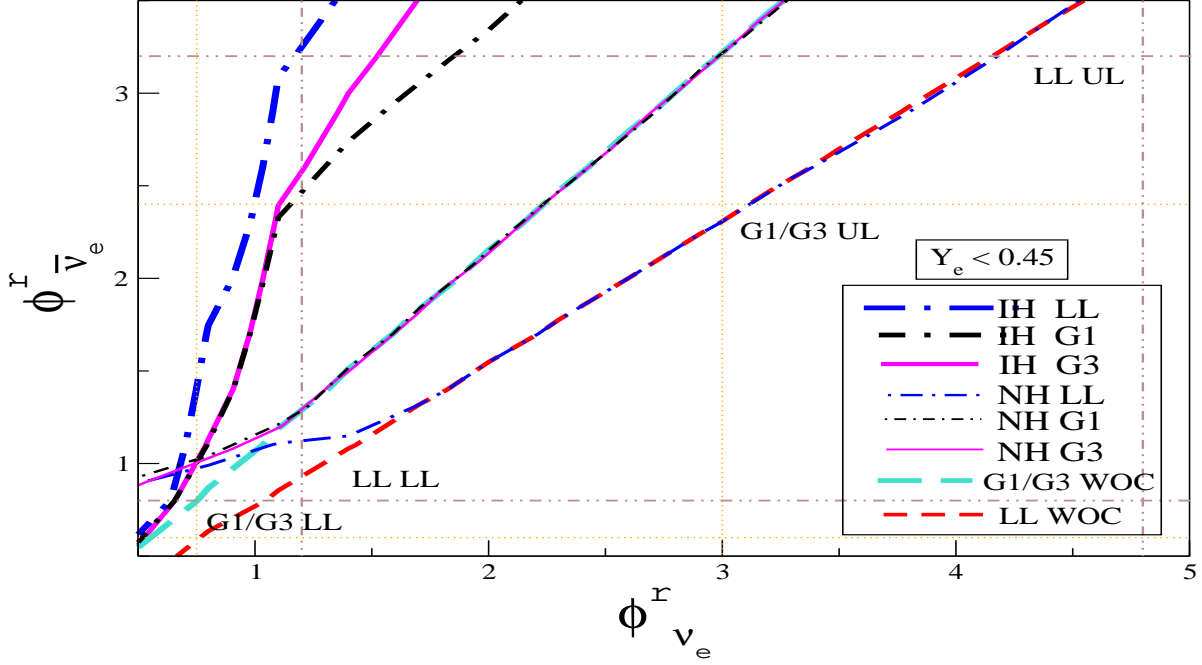


Figure 9: The exclusion plot consistent with  $Y_e < 0.45$  for the spectrum G1, G3 and LL for both NH and IH. The allowed area is to the left of the curves. The dotted orange lines denote the Lower Limit (LL) and Upper Limit (UL) of  $\phi_{\nu_e}^r$  and  $\phi_{\bar{\nu}_e}^r$  for G1 and G3, arising from the two fold uncertainty defined in Eq. (25). Similarly double dotted dashed brown lines denote the Lower Limit (LL) and Upper Limit (UL) for the Lawrence Livermore spectrum model (LL).

respective hierarchies) will not allow r-process once collective effects are taken into account and hence will be ruled out if one imposes the criteria that  $Y_e$  must be less than 0.5. Therefore, it is expected that the exclusion plot for any specific limit on  $Y_e$  will change once collective effects are taken into account.

In Figure 9 we show the exclusion plot in the  $\phi_{\nu_e}^r - \phi_{\bar{\nu}_e}^r$  plane for  $Y_e < 0.45$ . The lines themselves correspond to the case when  $Y_e = 0.45$ , while the allowed area (which gives  $Y_e < 0.45$  or  $\lambda_{\bar{\nu}_{ep}}/\lambda_{\nu_{en}} > 1.22$ ) is to the left of the curves. We reiterate that the survival probabilities for these plots have been calculated at  $r = 400$  km. We vary  $\phi_{\nu_e}^r$  and  $\phi_{\bar{\nu}_e}^r$  in the ranges (0.5,5.0) and (0.5,3.5) respectively. We plot exclusion curves for both IH and NH, and for all the three spectra models. We also plot the exclusion curves when collective oscillations are absent (WOC) for LL (thick red dashed) and G1/G3 (thick sky blue long dashed). These lines correspond to the no conversion case discussed earlier. We can see that they are almost straight lines in the  $\phi_{\nu_e}^r - \phi_{\bar{\nu}_e}^r$ , with  $\phi_{\nu_e}^r/\phi_{\bar{\nu}_e}^r = 1.22 * \langle (E + \Delta_{np})^2 \rangle_{\nu_e} / \langle (E - \Delta_{np})^2 \rangle_{\bar{\nu}_e}$ , for the respective spectral model. Since the average energy as well as the spectral shape (cf. Eq. (17)) for both G1 and G3 are the same, the exclusion lines for no oscillation case for them is identical. For LL, since the ratio of  $\langle (E + \Delta_{np})^2 \rangle_{\nu_e} / \langle (E - \Delta_{np})^2 \rangle_{\bar{\nu}_e}$  is smaller (0.62) than for G1/G3 (0.88), the exclusion line for no oscillation case for LL corresponds to smaller  $\phi_{\nu_e}^r/\phi_{\bar{\nu}_e}^r$ . We see from the figure that for NH the effect of collective oscillations are mainly in the low  $\phi_{\nu_e}^r$  and  $\phi_{\bar{\nu}_e}^r$  region. This conforms to the observation in section 2, where we had shown that the split energy increased with increasing  $\phi_{\nu_e}^r$  and/or  $\phi_{\bar{\nu}_e}^r$ . Since the flux begins to fall with increasing energy, the impact of collective oscillations fall for higher  $\phi_{\nu_e}^r$  and  $\phi_{\bar{\nu}_e}^r$ . Hence for

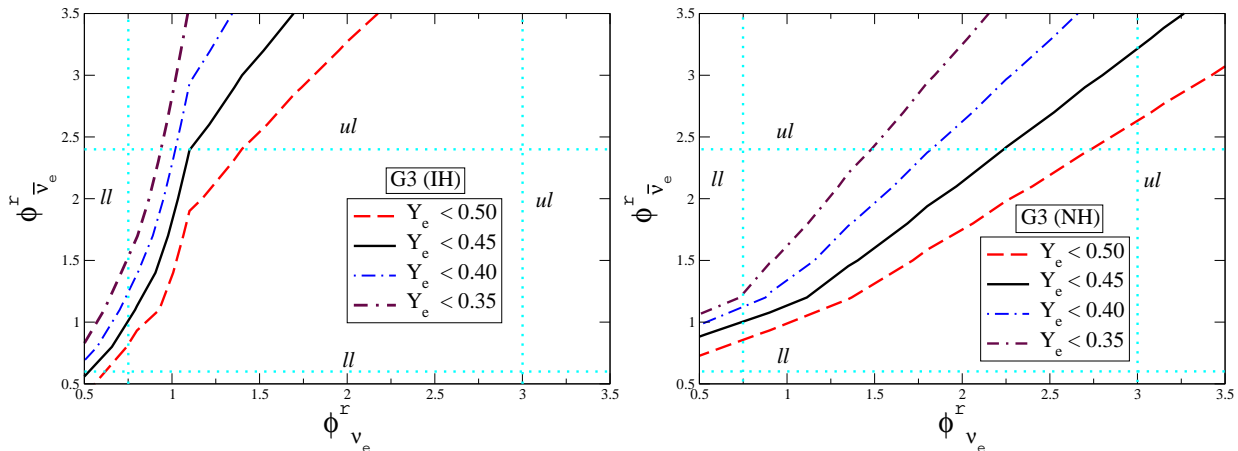


Figure 10: Exclusion plots for NH and IH for model G3. The exclusion condition is varied from  $Y_e < 0.35$  to 0.5. The dotted sky blue lines denote the ‘*ll*’ (Lower Limit) and ‘*ul*’ (Upper Limit) from the assumed two fold uncertainty of  $\phi_{\nu_e}^r$  and  $\phi_{\bar{\nu}_e}^r$ , for the spectrum model G3. The allowed region is on the left side of the exclusion curves.

all the three models, the NH exclusion curves at higher relative luminosities agree with the WOC ones, as there is no observed collective effect there. Whereas at lower relative luminosities the curves deviate from the WOC ones due to the observed single splits, making the allowed region smaller. Again, as seen in Figure 8, the effect of collective oscillations is to increase  $Y_e$  for any given  $\phi_{\bar{\nu}_e}^r/\phi_{\nu_e}^r$ . Since  $Y_e$  decreases with  $\phi_{\bar{\nu}_e}^r/\phi_{\nu_e}^r$ , the exclusion plots shift to larger  $\phi_{\bar{\nu}_e}^r/\phi_{\nu_e}^r$  values once collective oscillations are switched on. This results in the curves shifting left in the  $\phi_{\bar{\nu}_e}^r$ - $\phi_{\nu_e}^r$  plane.

Figure 9 shows that for IH, the effect of collective oscillations can be very significant in constraining the relative luminosities. This can be understood from Figures 7, 8 and Eq 31. In Figure 8 we see that the effect of collective oscillation is to shift  $Y_e$  to a higher value. Eq. 31 shows that this can be balanced by increasing  $\phi_{\bar{\nu}_e}^r$  compared to  $\phi_{\nu_e}^r$ . This results in shifting the contour plots to the left of the  $\phi_{\bar{\nu}_e}^r$  -  $\phi_{\nu_e}^r$  plane in Fig.9. Since Figures 7 and 9 show the same  $\phi_{\bar{\nu}_e}^r$ - $\phi_{\nu_e}^r$  plane, we can see that for IH once collective oscillations are switched on, the only region in this plane which remains allowed is the one where we have double splits in the neutrino sector and no splits in the antineutrino sector. This is the (II, 0) zone where  $J_z < 0$  and  $D_z < 0$ .

One understands that stronger constraint on  $Y_e$  reduces the allowed parameter space. Figure 10 shows the exclusion plots for IH and NH for the model G3 for various constraints  $Y_e < 0.35$ , 0.40, 0.45, 0.50. The left panel is for IH and the right one for NH. Since higher values of  $\phi_{\nu_e}^r$  gives higher  $Y_e$ , as one reduces the required value of  $Y_e$ ,  $\phi_{\nu_e}^r$  gets more constrained. The constraint on  $\phi_{\bar{\nu}_e}^r$  is relatively weak. But very low values of  $\phi_{\bar{\nu}_e}^r$  are not allowed as we have seen that lower values of  $\phi_{\bar{\nu}_e}^r$  increases the electron fraction.

Some final comments are in order. We would like to reiterate here that our analysis and the corresponding exclusion plots are meant as a proof of principle and merely indicate the ranges of the allowed fluxes for which one gets neutron-rich regions for r-process in the neutrino driven wind. They show that all r-process calculations should take collective effects into account and

such detailed simulations can be used to extract more rigorous bounds on the initial fluxes.

Now we discuss the evolution as a function of time and its implication for our results. Early times have larger luminosities and may deviate more from energy equipartition. In realistic simulations in the cooling phase the luminosity for each species decreases with time as mentioned earlier but it may be reasonable to assume that the relative luminosities change very slowly with respect to time. With time the shock moves out, the neutrinospheres slowly fall in, the matter in the hot bubble and the wind driven region cools and the constituents change, first producing alpha-particles and then heavier nuclei. The alpha particles are strongly bound systems and their excitation by  $\nu/\bar{\nu}$  can be neglected. The inclusion of  $\alpha$ -particles in the matter was considered in [47] and the effect of the nuclear composition involving heavier nuclei on  $Y_e$  was looked at in [16]. A similar study including spectral splits in a self-consistent manner for the time-evolved system need to be undertaken separately in future.

One also realizes that there are many uncertainties that exist presently in the occurrence of the r-process in the supernovae. Firstly large entropy needed for the development of the r-process, as mentioned earlier, need to be observed consistently in all one dimensional simulations as well as in simulations going beyond one dimension. The hot bubble region does have the problem of having lower entropy [52]. This is compounded by the inability of simulations to give rise to outgoing shocks with the right explosion energy. Often the physics understanding comes from the use of ‘semi-analytic models’ [52] that critically depend on the three quantities  $Y_e$ , the entropy and the dynamic timescale.

## 4 Summary and Conclusions

Collective flavor oscillations driven by neutrino-neutrino interaction at the very high density region of core collapse supernovae control the emitted flux of neutrinos of different flavors. In the process one or more swaps of flavors for both neutrinos and antineutrinos take place depending on the initial neutrino flux and distributions. We study the phenomena of spectral splits and consequent flavor swaps for different models of neutrino spectrum, varying the relative luminosities of neutrinos and antineutrinos for both normal and inverted mass hierarchy. The effect of spectral splits is found to be more pronounced for inverted hierarchy and depending on the initial luminosities one can get single or dual splits in neutrinos and/or antineutrinos. For a specific choice of relative luminosity we also find a case for inverted hierarchy where the splits are not resolvable numerically and is akin to no spectral splits for all practical purposes. Single split patterns are also obtained for normal hierarchy for some choices of the luminosities. Next we consider the impact of the collective oscillations and the spectral splits on the electron fraction  $Y_e$ , which determines if the environment is neutron-rich and compatible with r-process nucleosynthesis or not. The minimal requirement for r-process is the electron-to-nucleon ratio  $Y_e < 0.5$ , but a more favorable condition may be  $Y_e < 0.45/0.40$ . We consider the flavor evolution reduced to an effective two flavor model with oscillation between  $\nu_e$  and  $\nu_x$  and their antiparticles. The oscillation parameters are chosen as  $\Delta m^2 = 3 \times 10^{-3} \text{ eV}^2$  and a small effective mixing angle  $\theta = 10^{-5}$  in agreement with realistic 1 – 3 mixing. For these values of parameters the ordinary MSW resonances take place beyond the r-process region and hence there will be no effect of neutrino conversions on  $Y_e$  due to these. However, the inclusion of collective effects can affect the value of  $Y_e$  even for these values of mass and mixing parameters.

The electron fraction ( $Y_e$ ) as a function of the radius of the core is calculated and it shows an oscillatory behavior in the bipolar region due to collective effects, before saturating to a constant value which depends on the initial luminosities and the pattern of flavor swap. Different models of neutrino energy distributions are used. For each of the distributions initial fluxes of different flavors are varied and constraints on the initial neutrino fluxes consistent with successful r-process nucleosynthesis are shown in exclusion plots for these initial neutrino fluxes. While a detailed simulation of the r-process nucleosynthesis inside the supernova might bring some changes to the exclusion plots, this work illustrates the fact that such exclusion plots are possible to achieve.

The variation in the number of spectral splits with the variation in the luminosity give rise to different possibilities of neutrino and antineutrino spectrum at the detector. The constraints on luminosities obtained by ensuring r-process nucleosynthesis can provide additional inputs in narrowing down the possible patterns.

*Note added:* While this paper was under peer review, a few papers [56, 57] have appeared which study the possible effects of a three flavor treatment of the collective oscillations of supernovae neutrinos. The differences of this with a two flavor treatment and their impact on the r-process nucleosynthesis need to be investigated. However from the above studies it is expected that the extra effect due to three flavors may be observable in IH but the changes in NH will be minor.

## 5 Acknowledgments

S. Chakraborty wishes to thank Basudeb Dasgupta for useful discussions and acknowledges hospitality at Physical Research Laboratory and Harish-Chandra Research Institute during the development stage of this work. S. Choubey and S.G. acknowledge support from the Neutrino Project under the XIth plan of Harish-Chandra Research Institute. K.K acknowledges hospitality at The Institute of Mathematical Sciences. K.K and S. Chakraborty acknowledge support from the projects ‘Center for Astroparticle Physics’ and ‘Frontiers of Theoretical Physics’ of Saha Institute of Nuclear Physics.

## References

- [1] G. Raffelt, *Stars as Laboratories for Fundamental Physics* (U. of Chicago Press, Chicago, 1996), 664 pp.
- [2] A. Dighe, J. Phys. Conf. Ser. **136**, 022041 (2008).
- [3] L. Wolfenstein, *Phys. Rev.* **D17**, 2369 (1978); S.P. Mikheyev and A.Yu. Smirnov, *Sov. J. Nucl. Phys.* **42(6)**, 913 (1985); *Nuovo Cimento* **9c**, 17 (1986).
- [4] G. L. Fogli, E. Lisi, A. Mirizzi, and D. Montanino, *Phys. Rev. D* **68**, 033005 (2003) [hep-ph/0304056].
- [5] B. Dasgupta and A. Dighe, *Phys. Rev. D* **75** (2007) 093002 [hep-ph/0510219].
- [6] S. Choubey, N. P. Harries and G. G. Ross, *Phys. Rev. D* **74**, 053010 (2006) [hep-ph/0605255].

- [7] G. L. Fogli, E. Lisi, A. Mirizzi and D. Montanino, JCAP **0606**, 012 (2006) [hep-ph/0603033].
- [8] R.C.Schirato, G.M. Fuller, [astro-ph/0205390].
- [9] R. Tomas et al, JCAP 0409, 015 (2004)
- [10] J. T. Pantaleone, Phys. Lett. B **287**, 128 (1992).
- [11] G. Sigl and G. Raffelt, Nucl. Phys. B **406**, 423 (1993).
- [12] V. A. Kostelecky and S. Samuel, Phys. Rev. D **52**, 621 (1995).
- [13] S. Pastor, G. G. Raffelt and D. V. Semikoz, Phys. Rev. D **65**, 053011 (2002).
- [14] Y. Y. Y. Wong, Phys. Rev. D **66**, 025015 (2002).
- [15] A. B. Balantekin and Y. Pehlivan, J. Phys. G **34**, 47 (2007).
- [16] G. C. McLaughlin, G. M. Fuller and J. R. Wilson, Astrophys. J. **472**, 440 (1996) [arXiv:astro-ph/9701114].
- [17] S. Pastor and G. Raffelt, Phys. Rev. Lett. **89**, 191101 (2002).
- [18] R. F. Sawyer, Phys. Rev. D **72**, 045003 (2005).
- [19] H. Duan, G. M. Fuller and Y. Z. Qian, Phys. Rev. D **74**, 123004 (2006).
- [20] H. Duan, G. M. Fuller, J. Carlson and Y. Z. Qian, Phys. Rev. D **74**, 105014 (2006).
- [21] S. Hannestad, G. G. Raffelt, G. Sigl and Y. Y. Y. Wong, Phys. Rev. D **74**, 105010 (2006); Erratum ibid. **76**, 029901 (2007).
- [22] G. G. Raffelt and G. Sigl, Phys. Rev. D **75**, 083002 (2007).
- [23] A. Esteban-Pretel *et al.*, Phys. Rev. D **76**, 125018 (2007).
- [24] H. Duan, G. M. Fuller, J. Carlson and Y. Z. Qian, Phys. Rev. D **75**, 125005 (2007).
- [25] G. G. Raffelt and A. Yu. Smirnov, Phys. Rev. D **76**, 081301 (2007); Erratum ibid. **77**, 029903 (2008).
- [26] G. G. Raffelt and A. Yu. Smirnov, Phys. Rev. D **76**, 125008 (2007).
- [27] H. Duan, G. M. Fuller and Y. Z. Qian, Phys. Rev. D **76**, 085013 (2007).
- [28] H. Duan, G. M. Fuller, J. Carlson and Y. Z. Qian, Phys. Rev. Lett. **99**, 241802 (2007).
- [29] G. L. Fogli, E. Lisi, A. Marrone and A. Mirizzi, JCAP **0712**, 010 (2007).
- [30] G. L. Fogli *et al.*, Phys. Rev. D **78**, 097301 (2008).
- [31] H. Duan, G. M. Fuller, J. Carlson and Y. Z. Qian, Phys. Rev. Lett. **100**, 021101 (2008).

- [32] B. Dasgupta, A. Dighe, A. Mirizzi and G. G. Raffelt, Phys. Rev. D **77**, 113007 (2008).
- [33] B. Dasgupta and A. Dighe, Phys. Rev. D **77**, 113002 (2008).
- [34] H. Duan, G. M. Fuller and Y. Z. Qian, Phys. Rev. D **77**, 085016 (2008).
- [35] B. Dasgupta, A. Dighe and A. Mirizzi, Phys. Rev. Lett. **101**, 171801 (2008).
- [36] A. Esteban-Pretel *et al.*, Phys. Rev. D **78**, 085012 (2008).
- [37] B. Dasgupta, A. Dighe, A. Mirizzi and G. G. Raffelt, Phys. Rev. D **78**, 033014 (2008) [arXiv:0805.3300].
- [38] J. Gava and C. Volpe, Phys. Rev. D **78**, 083007 (2008).
- [39] G. G. Raffelt, Phys. Rev. D **78**, 125015 (2008). 72
- [40] G. Fogli, E. Lisi, A. Marrone and I. Tamborra, JCAP **0904**, 030 (2009) [arXiv:0812.3031 [hep-ph]].
- [41] B. Dasgupta, A. Dighe, G. G. Raffelt and A. Y. Smirnov, Phys. Rev. Lett. **103**, 051105 (2009) [arXiv:0904.3542 [hep-ph]].
- [42] G. Fogli, E. Lisi, A. Marrone and I. Tamborra, arXiv:0907.5115 [hep-ph].
- [43] S. Chakraborty, S. Choubey, B. Dasgupta and K. Kar, JCAP **0809**, 013 (2008) [arXiv:0805.3131 [hep-ph]].
- [44] C. Lunardini Phys. Rev. Lett. **102**, 231101 (2009) [arXiv:0901.0568 [astro-ph.SR]]
- [45] H. Duan and James P Kneller J. Phys. **G36**, 113201 (2009). [arXiv:0904.0974 [astro-ph.HE]]
- [46] Y. Z. Qian, G. M. Fuller, G. J. Mathews, R. Mayle, J. R. Wilson and S. E. Woosley, Phys. Rev. Lett. **71**, 1965 (1993).
- [47] A. B. Balantekin and H. Yuksel New J. Phys. **7**, 51 (2005). [astro-ph/0411159]
- [48] T. Totani, K. Sato, H. E. Dalhed, J. R. Wilson, Astrophys. J. 496,216 (1998) [astro-ph/9710203],
- [49] T. A. Thompson, A. Burrows, P. Pinto, Astrophys. J. 592,434 (2003). [astro-ph/0211194]
- [50] M. T. Keil, G. G. Raffelt and H. T. Janka, Astrophys. J. **590**, 971 (2003) [arXiv:astro-ph/0208035].
- [51] C. Lunardini and A. Yu. Smirnov, JCAP **0306**, 009 (2003) [hep-ph/0302033].
- [52] For a recent review M. Arnould, S. Goriely and K. Takahashi, Phys. Rep.**450** 97-213 (2007).
- [53] H.A.Bethe and J.R.Wilson, Astrophys. J. **295**, 14 (1985).

- [54] James P. Kneller, Gail C. McLaughlin Phys. Rev. D **80**, 053002 (2009).
- [55] A. Esteban-Pretel *et al.*, Phys. Rev. D **77**, 065024 (2008).
- [56] A. Friedland, [arXiv:1001.0996 [hep-ph]]
- [57] B. Dasgupta *et al.* [arXiv:1002.2943 [hep-ph]]